

Probing the effects of lithium doping on structures, properties, and stabilities of magnesium cluster anions

Xiao-Yi Zhang(张小义), Ya-Ru Zhao(赵亚儒), Hong-Xing Li(李红星), Kai-Ge Cheng(成凯格), Zi-Rui Liu(刘子锐), Zhi-Ping Liu(刘芷萍), and Hang He(何航)

Citation: Chin. Phys. B, 2023, 32 (**6**): 066102. DOI: 10.1088/1674-1056/acc51f
Journal homepage: http://cpb.iphy.ac.cn; http://iopscience.iop.org/cpb

What follows is a list of articles you may be interested in

Effects of atomic corrugations on electronic structures in $Pb_{1-x}Bi_x$ thin films

Pengju Li(李鹏举), Kun Xie(谢鹍), Yumin Xia(夏玉敏), Desheng Cai(蔡德胜), and Shengyong Qin(秦胜勇)
Chin. Phys. B, 2023, 32 (**6**): 066101. DOI: 10.1088/1674-1056/acbf29

Pressure-induced stable structures and physical properties of Sr-Ge system

Shuai Han(韩帅), Shuai Duan(段帅), Yun-Xian Liu(刘云仙), Chao Wang(王超), Xin Chen(陈欣), Hai-Rui Sun(孙海瑞), and Xiao-Bing Liu(刘晓兵)
Chin. Phys. B, 2023, 32 (**1**): 016101. DOI: 10.1088/1674-1056/ac6db5

Core structure and Peierls stress of the 90° dislocation and the 60° dislocation in aluminum investigated by the fully discrete Peierls model

Hao Xiang(向浩), Rui Wang(王锐), Feng-Lin Deng(邓凤麟), and Shao-Feng Wang(王少峰)
Chin. Phys. B, 2022, 31 (**8**): 086104. DOI: 10.1088/1674-1056/ac587f

Temperature dependence of bismuth structures under high pressure

Xiaobing Fan(范小兵), Shikai Xiang(向士凯), and Lingcang Cai(蔡灵仓)
Chin. Phys. B, 2022, 31 (**5**): 056101. DOI: 10.1088/1674-1056/ac398d

Evolution of defects and deformation mechanisms in different tensile directions of solidified lamellar Ti-Al alloy

Yutao Liu(刘玉涛), Tinghong Gao(高廷红), Yue Gao(高越), Lianxin Li(李连欣), Min Tan(谭敏), Quan Xie(谢泉), Qian Chen(陈茜), Zean Tian(田泽安), Yongchao Liang(梁永超), and Bei Wang(王蓓)
Chin. Phys. B, 2022, 31 (**4**): 046105. DOI: 10.1088/1674-1056/ac1f0b

---

Probing the effects of lithium doping on structures, properties, and stabilities of magnesium cluster anions

Xiao-Yi Zhang(张小义), Ya-Ru Zhao(赵亚儒)†, Hong-Xing Li(李红星), Kai-Ge Cheng(成凯格), Zi-Rui Liu(刘子锐), Zhi-Ping Liu(刘芷萍), and Hang He(何航)

College of Physics and Optoelectronics Technology, Baoji University of Arts and Sciences, Baoji 721016, *China*

(Received 24 October 2022; revised manuscript received 14 February 2023; accepted manuscript online 17 March 2023)

Bimetallic clusters have aroused tremendous interest because the property changes like structure, size, and composition have occurred. Herein, a structural search of the global minimum for anionic $LiMg_n^-$ ($n = 2$–11) clusters is performed using an efficient crystal structure analysis by particle swarm optimization (CALYPSO) structural searching program with subsequent density functional theory (DFT) calculations. A great variety of low energetic isomers are converged, and the most stable ones are confirmed by comparing their total energy of each size. It is found that the $LiMg_n^-$ clusters are structurally consistent with corresponding Mg clusters anions except for $LiMg_5^-$ and $LiMg_7^-$. In all the doped clusters, the Li atom prefers to occupy the convex position. Simulated photoelectron spectra (PES), Infrared (IR), and Raman spectra of $LiMg_n^-$ could be used as an essential evidence for identifying cluster structures experimentally in the future. Stability study reveals that a tower-like structure of $LiMg_9^-$ has prominent stability and can be identified as a magic number cluster. The reason might be that there are both closed-shell $1S^2 1P^6 1D^{10} 2S^2$ electronic configurations and stronger Li–Mg bonds caused by sp hybridization in the $LiMg_9^-$ cluster.

Keywords: $LiMg_n^-$ clusters, crystal structure analysis by particle swarm optimization (CALYPSO), structures, electronic properties

PACS: 61.46.Bc **DOI:** 10.1088/1674-1056/acc51f

1. Introduction

As an intermediate transition state from atoms to bulk metals and alloys, metal clusters have novel physical and chemical properties different from bulk, which are associated with structure, size, and composition of clusters.[1–6] Therefore, scientists have tried to design metal clusters with high stability and excellent property as assembly units for developing new functional materials. After decades of research, a large number of metal clusters with outstanding properties have been found, such as Au_{20},[7] Al_{13}^-,[8] Fe_{55},[9] Pt_{10}^-,[10] and VNa_8.[11]

Magnesium-based metal clusters aroused a great deal of attention due to their superior advantages in hydrogen storage. Previous studies looked at many different aspects of magnesium clusters: nonmetal-to-metal transition, structures, magic numbers, and dopant effects on the properties and geometries. For example, the earliest experimental works reported the transition points of the nonmetal-to-metal transition were 20 and 18 for neutral and anionic magnesium clusters, respectively.[12,13] The structures of the small-sized Mg clusters had been carried out by abundant theoretical studies in the last few decades.[14–20] Because of the s and p orbitals interaction, their geometries easily form a compact structure. The magic numbers $N = 4$, 10, and 20 present in these clusters can be perfectly explained by using the spherical Jellium model.[21] Numerous binary clusters are accordingly found to have excellent properties by doping Mg clusters with foreign atoms,[22–27] such as magnetic superatoms $TMMg_8$ (TM = Fe, Co, Ni, and Tc),[28,29] efficient catalysts $TMMg_{55}$ (TM = Ti and Nb),[30] high stability cage $BeMg_{16}$ cluster,[31] and so on. To some extent, these experimental and theoretical results are significant for the enrichment of magnesium-based clusters.

Alkaline metal lithium, the most active and lightest metal, is extensively used in lithium cells, rocket fuel, fluxing agent, alloys, atomic reactors, etc. In particular, the Mg–Li alloy is the lightest metal structure material in the world, with good ductility, corrosion resistance, electrical and thermal conductivity, and widespread application.[32,33] The Mg–Li alloy is formed by the incorporation of 14%–16% lithium into close-packed hexagonal magnesium, resulting the original structure being transformed into a tetragonal one. A question arises: how the structures and properties of the host clusters are altered due to the loading of the foreign atom. For the Li–Mg binary clusters, there have several important studies for small-size clusters. The earliest theoretical studies appeared in 1988, in which the geometries and electronic structures of the Li_nMg ($n = 1$–7) clusters were investigated by Rao and Jena.[34] They pointed out that the geometries of the Li clusters can be modified significantly by the doping of Mg. Then, Fantucci *et al.*[35] performed an *ab initio* configuration interaction study of the $MgLi_k$ ($k = 2$–8) clusters and found that the Mg atom occupies the central position in the most stable structure except for $MgLi_3$. In the study of Deshpande *et al.*,[36] the eight valence

†Corresponding author. E-mail: bjwl_zyr@163.com

© 2023 Chinese Physical Society and IOP Publishing Ltd

electrons of the Li_6Mg cluster were proved to have the highest stability in the size range of $n = 1$–12 for Li_nMg clusters. Recently, a systematic investigation of structural and electronic properties of $LiMg_n$ ($n = 2$–11) clusters has been done by Li *et al.*[37] based on the DFT calculations. They found that the geometries of $LiMg_n$ are consistent with those of the pure Mg clusters at small size, while they are different at the large size. In addition, the stabilities of the host cluster were enhanced because the doped Li forms stronger Li–Mg bonds with the surrounding Mg atoms. Subsequently, Liu *et al.*[38] created the Mg_n clusters doped with two Li atoms. The results clearly showed that the foreign Li atoms induce noticeable effects on the structures and stabilities of the host clusters. Two magic number structures, Li_2Mg_3 and Li_2Mg_9, were proved to have $1S^21P^6$ and $1S^21P^61D^{10}2S^2$ closed-shell electronic configurations, in conformity with the spherical Jellium model. Although extensive studies are reported for Li–Mg binary clusters, these works have mainly focused on neutral clusters, and the anionic Li–Mg clusters studies are still lacking. In this article, we describe a systematic structure search for low-energy isomers of $LiMg_n^-$ clusters with up to 12 atoms by utilizing a global search technique. The structures, stabilities, and properties of $LiMg_n^-$ have been discussed. Our original motivations are as follows. (i) It will give us a comprehensive understanding of the geometries for anionic $LiMg_n$ clusters. (ii) Analysis of electronic nature and bonding character will supply valuable insight into microscopic mechanisms in binary metal clusters. (iii) We hope the study is helpful in developing new functional materials based on metal cluster assembly.

2. Computational methods

The low-lying structures of $LiMg_n^-$ and Mg_n^- are searched by the particle swarm optimization (PSO) algorithm implanted in the CALYPSO code,[39–41] which can efficiently explore the global minima structures on potential energy surfaces. In cluster structure prediction, many studies have successfully revealed its validity.[42–50] For each cluster size, there are more than 800 structurally different isomers located at 20 generations. It provides 50 structures in each generation, 70% of which are generated by PSO and the rest are newly produced. The trial structures are entirely performed for initial optimization using the Gaussian09 package[51] at B3PW91/6-31G level.[52] By comparing their total energies, we select isomers with 3 eV of energy difference compared with the most stable one for re-optimization at B3PW91/6-311 + G(d) level.[53,54] Frequency calculations are also performed simultaneously to make sure their true minimum. Different values of spin multiplicity (up to septet and octet) are considered in structure optimization, resulting in the most stable ones favoring the lowest spin states for the $LiMg_n^-$ and Mg_{n+1}^- clusters. Multiwfn software[55] is employed to obtain the results of bonding nature as well as IR and Raman spectra of the said clusters. Based on the Koopmans' theorem,[56] we simulate the PES of the most stable Mg_n^- and $LiMg_n^-$ clusters.

3. Results and discussion

3.1. Geometric structures

In the process of structural prediction, the ground state ones of anionic Mg clusters are quickly obtained, as shown in the first column of Fig. 1. Note that they are consistent with the results given in previous studies,[14–20] suggesting a reasonable method and computational level in this work. In addition, a comprehensive comparison between Mg_{n+1}^- and $LiMg_n^-$ will be carried out to elucidate the effect of Li doped on structures, stabilities, and properties of the host clusters.

Through the systematic structure search for $LiMg_n^-$ ($n = 2$–11) clusters, the most stable ones are verified, as presented in the second column of Fig. 1. Their electronic states and symmetries are tabulated in Table 1. The coordinates of atoms of the most stable $LiMg_n^-$ ($n = 2$–11) clusters are list in Table S1 (supplementary materials). Meanwhile, two or three typical isomers with low energy are exhibited for each size. One can find from Fig. 1 that most of the $LiMg_n^-$ clusters can be regarded as the substituted structures of pure Mg_{n+1}^- clusters, in which the convex position magnesium atoms are replaced by lithium atoms. For $LiMg_n^-$, the structural evolution shows a sequence of triangular bipyramid-, pentagonal bipyramid-, and trigonal prism-based motifs as the cluster size increases. Only Mg_3^- and $LiMg_2^-$ are two-dimensional structures. The $LiMg_2^-$ cluster has two linear metastable isomers with energy differences of 5.18 kcal/mol and 6.00 kcal/mol compared to 2a. Structural transition from the planar to three-dimension takes place at $LiMg_3^-$. The most stable $LiMg_3^-$ cluster (3a) with triangular pyramid motif is a substituted structure of Mg_4^-. The lowest energy of 2D isomer (3b) and 1D one (3c) is respectively 15.06 kcal/mol and 21.53 kcal/mol higher in energy than 3a. For $LiMg_4^-$, isomers 4a and 4b are substituted structures of the Mg_5^- cluster with triangular bipyramid geometry. Indeed, they can be generated by capping one Mg atom on the 3a structure. The 4c isomer is derived from the Mg_4^- structure by adding one Li on the top. The lowest energy 2D isomer (4d) is yielded after capping an Mg atom on 3b. The Mg_6^- cluster has a pretty pentagonal pyramid structure (C_{5v} symmetry), however, no substituted structure is found in $LiMg_5^-$. The most stable isomer 5a is a boat-shaped structure, generated by adding an Mg atom on 4a. The other boat-like isomer 5b comes from 4b. Isomers 5c and 5d with a triangular bipyramid-based motif are derived from 4b and 4c structures. By comparing the energies, they are respectively 4.02 kcal/mol, 9.86 kcal/mol, and 10.98 kcal/mol higher than 5a. As two substituted structures of Mg_7^-, isomer

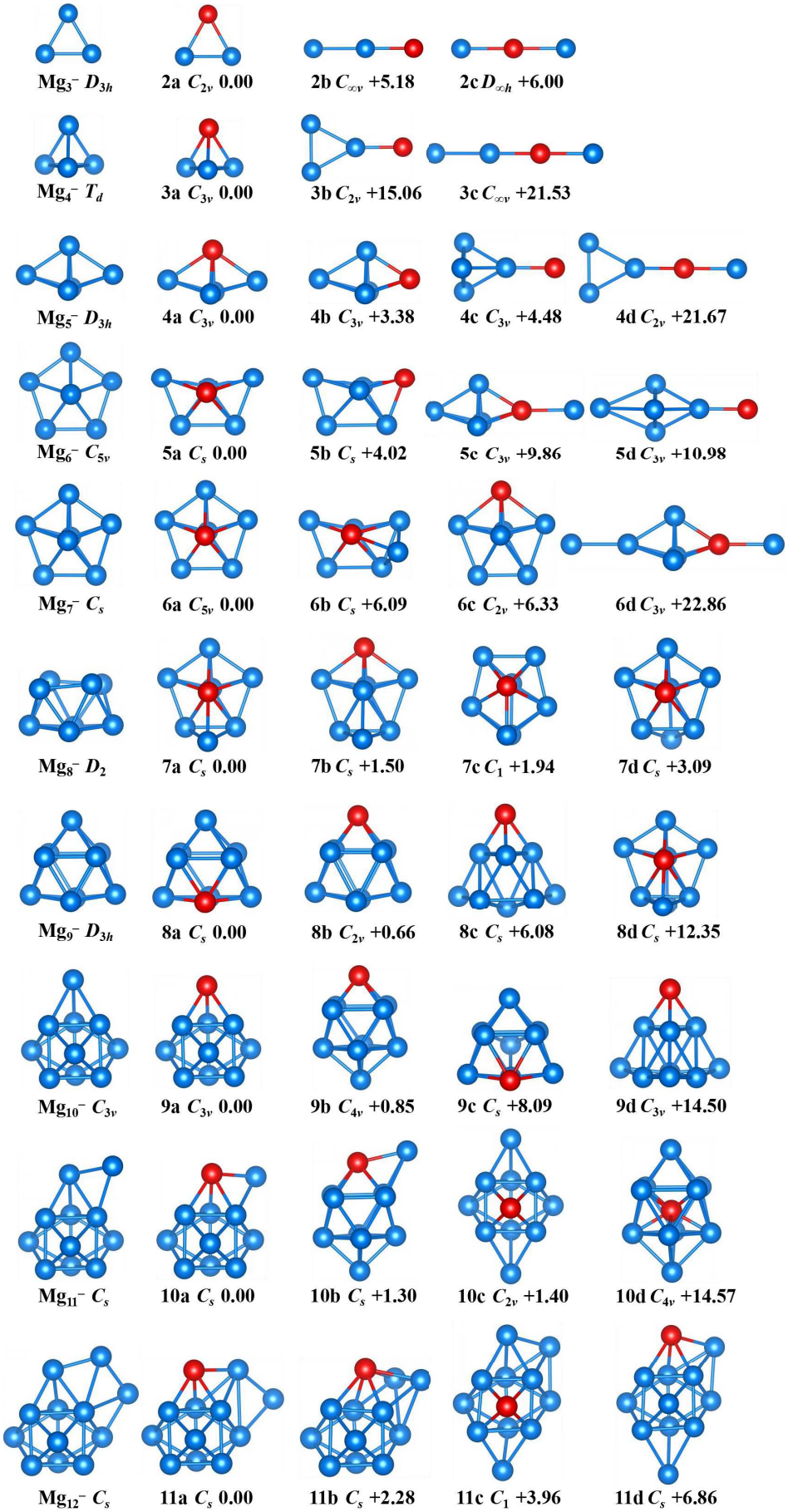


Fig. 1. The most stable structures of the Mg_{n+1}^- and $LiMg_n^-$ ($n = 2$–11) clusters as well as several typical low-lying isomers (energy difference in kcal/mol) of the $LiMg_n^-$ clusters.

Table 1. Electronic states, symmetries, average binding energies E_b (eV), fragmentation energy E_f (eV), second-order energy difference Δ^2E (eV), HOMO–LUMO energy gaps E_g (eV), frequency (cm^{-1}), and vertical detachment energy (VDE) of the most stable $LiMg_n^-$ ($n = 2$–11) clusters.

Clusters	Sta.	Sym.	E_b	E_f	Δ^2E	E_g	Lowest frequency	Highest frequency	VDE
$LiMg_2^-$	$^1A_1$	C_{2v}	0.544	–	–	1.291	140	191	0.93
$LiMg_3^-$	$^1A_1$	C_{3v}	0.671	1.052	0.451	1.354	158	243	1.23
$LiMg_4^-$	$^1A_1$	C_{3v}	0.657	0.602	0.035	1.564	77	267	1.46
$LiMg_5^-$	$^1A'$	C_s	0.642	0.567	−0.365	1.552	56	268	1.70
$LiMg_6^-$	$^1A_1$	C_{5v}	0.684	0.932	0.334	1.570	98	270	1.79
$LiMg_7^-$	$^1A'$	C_s	0.673	0.598	−0.477	1.452	56	227	1.93
$LiMg_8^-$	$^1A'$	C_s	0.718	1.075	−0.351	1.029	87	274	1.77
$LiMg_9^-$	$^1A_1$	C_{3v}	0.788	1.426	1.046	1.937	81	296	1.97
$LiMg_{10}^-$	$^1A'$	C_s	0.751	0.380	−0.232	1.347	42	288	1.83
$LiMg_{11}^-$	$^1A'$	C_s	0.740	0.612	–	1.365	28	293	1.97

6a with C_{5v} symmetry has a highly coordinated Li atom, resulting in it being an energy advantage over 6c. The 6b and 6d isomers are derived from 5a and 5c after an Mg atom is capped on them. The Mg_8^- and $LiMg_7^-$ clusters are entirely different configurations. Mg_8^- shows a square antiprism, but $LiMg_7^-$ displays a triangular bipyramid-based structure. From $n = 8$, the most stable structures of $LiMg_n^-$ display not only a trigonal prism-based geometry but also the same configurations as the corresponding Mg_n^- clusters. As for $LiMg_8^-$, two substituted isomers (8a and 8b) are formed when one Li atom replaces Mg in two different positions of Mg_9^-. The 8c isomer is a new shape with an energy of 6.08 kcal/mol compared to 8a. Isomers 8d is yielded from the previous 7a isomer. There are three highly symmetrical structures for the $LiMg_9^-$ cluster, including 9a with C_{3v} symmetry, 9b with C_{4v} symmetry, and 9d with C_{3v} symmetry. In energetic competition, isomers 9b and 9d are not superior to a substituted structure (9a) of Mg_{10}^-. When a vertex Mg atom of Mg_{11}^- is replaced by a Li atom, the most stable $LiMg_{10}^-$ cluster is produced. Of course, it can be generated by capping an Mg atom on the side of 9a. After two Mg atoms are symmetrically capped on 8b, isomer 10c is yielded. It is interesting to find a filled cage structure (10d) with an interior Li atom in the $LiMg_{10}^-$ cluster, which is just a metastable isomer. Isomers 11a, 11b, and 11d come from the most stable $LiMg_{10}^-$ cluster when an Mg atom is capped on different sites of 10a. The 11c isomer is derived from the 10c structure. Their energy differences compared to 11a are 2.28 kcal/mol, 3.96 kcal/mol, and 6.86 kcal/mol, respectively. Finally, we find that the structures of the most stable $LiMg_n^-$ clusters are inconsistent with $LiMg_n$ reported by Li *et al.*[37] except for $n = 2$ and 3, which indicates that the extra charge has a significant influence on the structures of Li-doped Mg_n clusters.

3.2. Photoelectron spectra (PES) of Mg_n^- and $LiMg_n^-$ clusters

As we know, for anionic clusters, an effective way to confirm their ground state structure is performing a comparison of theoretical photoelectron spectra (PES) with the experimental ones. Based on the most stable Mg_n^- clusters of our optimization, the simulated PES of Mg_n^- are displayed in Fig. 2 compared to experimental PES.[13] An excellent agreement validates that the global minimum structure obtained by PSO algorithm and our computational level is reliable. Although the PES of $LiMg_n^-$ are lacking in experiments, we hope that the theoretical PES can provide a valuable reference for identifying their ground state structures in the future. For the $LiMg_n^-$ clusters in detail, the electron binding energy of the first peak in PES curve corresponds to the value of the vertical detachment energy (VDE), which represents the energy required to strip an electron vertically from anionic clusters. Clusters with lower VDE are less thermal stable, while those with higher VDE are more thermal stable. The calculated values of VDE are listed in Table 1. For both $LiMg_2^-$ and $LiMg_3^-$ clusters, there are two visible peaks at 0.93 eV/2.16 eV and 1.23 eV/2.34 eV, respectively. It is found that the VDE (0.93 eV) of $LiMg_2^-$ is the smallest one for the $LiMg_n^-$ clusters, indicating the lowest thermal stability. As for $LiMg_4^-$, three discrete peaks at 1.46 eV, 2.01 eV, and 2.64 eV are observed in the PES. Since the structure of Mg_6^- and $LiMg_5^-$ is quite different, their PES contours are divergent. One can find a shoulder peak in the PES of the $LiMg_5^-$ cluster, in which three peaks have the position of 1.70 eV, 1.97 eV, and 2.47 eV. The PES of $LiMg_6^-$ contains a minor peak of 1.79 eV and two higher peaks of 2.25 eV and 2.70 eV. For the $LiMg_7^-$ cluster, the first peak locates at 1.93 eV, followed by a minor peak at 2.16 eV and a higher peak at 2.48 eV. In contrast, there are similar PES shapes for both $LiMg_{8-11}^-$ and Mg_{9-12}^- clusters in every size due to their identical geometries. A total of three peaks are observed at 1.77 eV, 2.36 eV, and 2.63 eV in the PES of $LiMg_8^-$. The PES of $LiMg_9^-$ are also composed of three peaks at 1.97 eV, 2.45 eV, and 2.61 eV. The most considerable VDE value of 1.97 eV means a more thermal stable of $LiMg_9^-$ in the said cluster size range. For $LiMg_{10}^-$, its PES contain four peaks at 1.83 eV, 2.41 eV, 2.68 eV, and 2.86 eV. In the PES of $LiMg_{11}^-$, the first peak appears at 1.97 eV, followed by a peak at 2.35 eV and a doublet peak at 2.63 eV/2.85 eV.

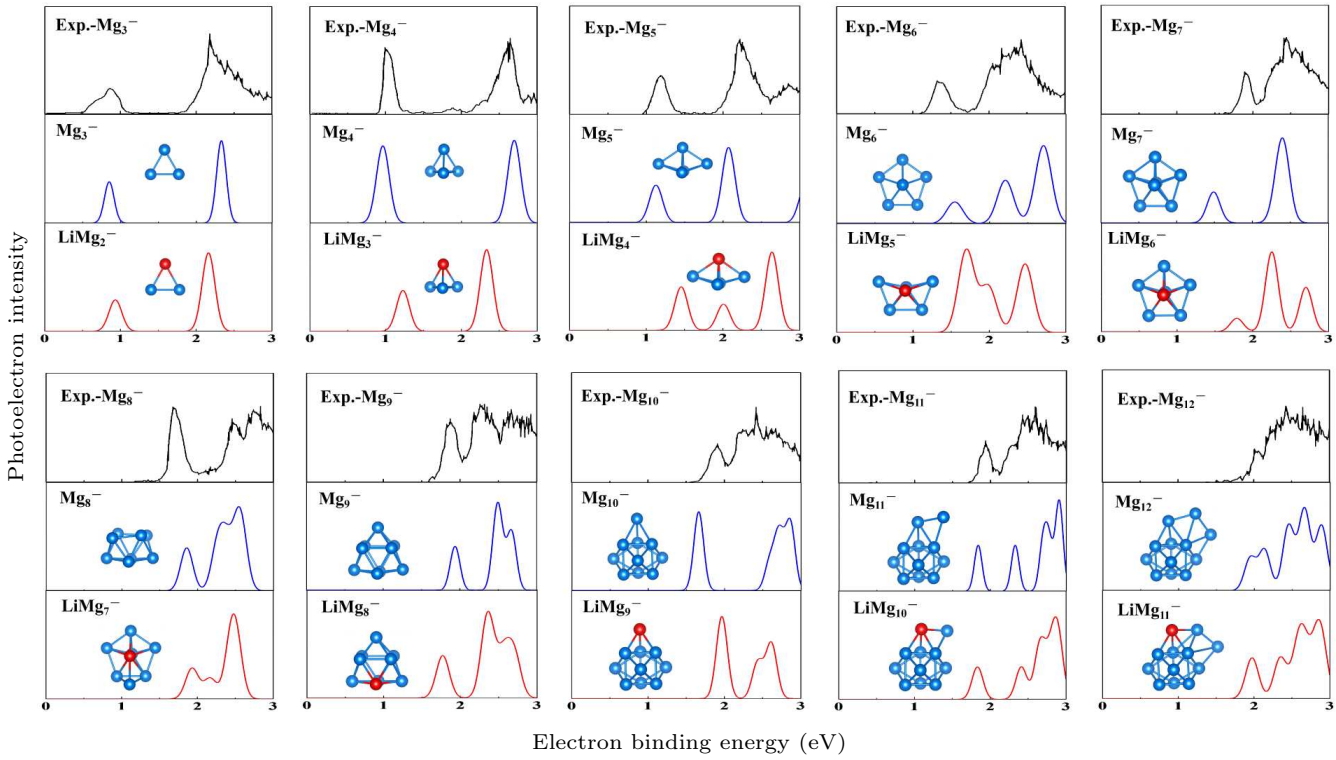


Fig. 2. Simulated PES of the most stable Mg_{n+1}^- and $LiMg_n^-$ ($n = 2$–11) clusters compared with experimental results of the Mg_{n+1}^- clusters.

3.3. Thermodynamic stability and HOMO–LUMO gap

The average binding energy (E_b in eV), fragmentation energy (E_f in eV), and second-order energy difference (Δ^2E in eV) are calculated for Mg_n^- and $LiMg_n^-$ to clarify the thermodynamic stability, which are defined as follows:

$$E_b(Mg_n^-) = \frac{(n-1)E(Mg)+E(Mg^-)-E(Mg_n^-)}{n}, \quad (1)$$

$$E_b(LiMg_n^-) = \frac{(n-1)E(Mg)+E(Mg^-)+E(Li)-E(LiMg_n^-)}{n+1}, \quad (2)$$

$$E_f(Mg_n^-) = E(Mg_{n-1}^-)+E(Mg)-E(Mg_n^-), \quad (3)$$

$$E_f(LiMg_n^-) = E(LiMg_{n-1}^-)+E(Mg)-E(LiMg_n^-), \quad (4)$$

$$\Delta^2E(Mg_n^-) = E(Mg_{n-1}^-)+E(Mg_{n+1}^-)-2E(Mg_n^-), \quad (5)$$

$$\Delta^2E(LiMg_n^-) = E(LiMg_{n-1}^-)+E(LiMg_{n+1}^-)-2E(LiMg_n^-), \quad (6)$$

where E denotes the energy of the corresponding clusters or atoms. The calculated results as the cluster size increases are depicted in Fig. 3 and the values of $LiMg_n^-$ are collected in Table 1. As Fig. 3(a) displayed, overall, the values of E_b increase non-monotonically as the size grows, indicating that the atoms within larger-size clusters bind more stably for said clusters. In contrast, the $LiMg_n^-$ clusters have enormous binding energies of 0.544 eV–0.788 eV, slightly larger than those (0.447 eV–0.710 eV) of corresponding Mg_{n+1}^- clusters, which means that the stability of the magnesium clusters can be enhanced by Li atom doping. Four dominant spots can be found at $n = 3$ and 9 for $LiMg_n^-$ and $n = 3$ and 8 for Mg_{n+1}^-, suggesting higher stability of the $LiMg_{3,9}^-$ and $Mg_{4,9}^-$ clusters. The magic numbers 3 and 9 are interesting for the $LiMg_n^-$ clusters. It is well known that $n = 3$ and 9 correspond to closings of atomic shells with 8 and 20 valence electrons. In Figs. 3(b) and 3(c), the curves of the E_f and Δ^2E exhibit irregular oscillations along with several localized maxima of $LiMg_3^-$, $LiMg_6^-$, and $LiMg_9^-$. It indicates more stability of them than their neighboring clusters. The high stability of $LiMg_6^-$ can be explained by the deformed Jellium model,[57,58] which applies to a spheroidal Jellium cluster. It demonstrates that the spheroidal Jellium clusters with 6, 10, 14, 22, 26, 30, etc., valence electrons turn out to be relatively stable. The $LiMg_6^-$ cluster satisfies this situation. In particular, outstanding stability can be shown for the $LiMg_9^-$ cluster because of its largest E_f and Δ^2E values.

In cluster science, the HOMO–LUMO gap (E_g in eV) is regarded as an essential indicator to depict their chemical stability. A larger E_g value signifies that it takes more energy to make its electron jumps from an occupied orbital to an unoccupied one. That corresponds to a more chemical stability cluster. Here, the size-induced variations of E_g for both Mg_n^- and $LiMg_n^-$ clusters are depicted in Fig. 3(d). As we can see, the values of Mg_n^- keep in a relatively stable range, but those of $LiMg_n^-$ have more significant fluctuations. In most cases, the $LiMg_n^-$ clusters own considerable E_g value, evidently higher than Mg_{n+1}^-, exhibiting more chemical stability. Interestingly, a prominent peak of 1.937 eV for the $LiMg_9^-$ cluster supports its higher chemical stability in said cluster range.

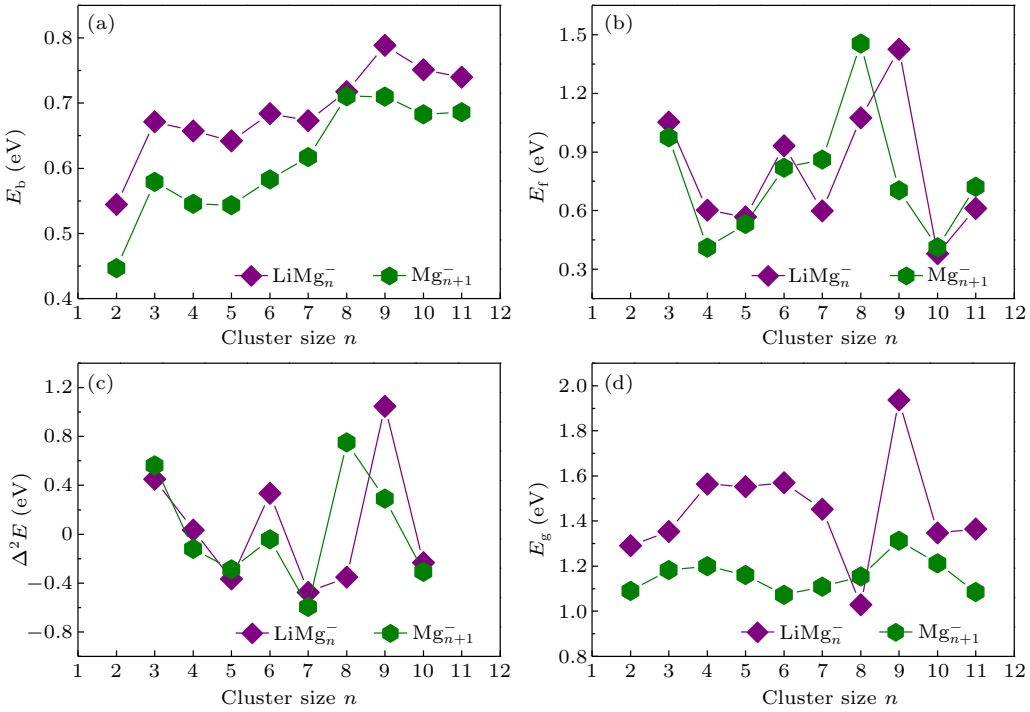


Fig. 3. Size dependence of (a) the average binding energy E_b, (b) fragmentation energy E_f (eV), (c) second-order energy difference Δ^2E, and (d) HOMO–LUMO gaps E_g for the Mg_{n+1}^- and $LiMg_n^-$ ($n = 2$–11) clusters.

3.4. Charge transfer

The natural population analysis (NPA) and natural electronic configuration (NEC) can clarify charge transfer behavior and provide more detailed information on each atomic orbital of clusters. In Table 2, we list the charges on Li atoms as well as electronic configurations on each atomic orbital of the Li and Mg atoms. Since each of these $LiMg_n^-$ clusters has an extra negative charge, it spreads over the Li and Mg atoms in $LiMg_2^-$, $LiMg_3^-$, $LiMg_7^-$, and $LiMg_8^-$ clusters. However, the charge distribution is different in the remaining clusters. In $LiMg_{4-6,9-11}^-$, the extra charge is not only given to the Mg atoms, but also some of the charges on Li atom are transferred to the surrounding Mg atoms due to all positive charges on Li atoms in them. For all of the $LiMg_n^-$ clusters, the internal charge transfer from s to p orbitals occurs, signifying the presence of sp hybridization in said clusters.

Table 2. The charges on the Li atoms and natural electronic configuration (NEC) of the $LiMg_n^-$ ($n = 2$–11) clusters.

Clusters	Charge on Li	NEC	
		Li	Mg
$LiMg_2^-$	−0.291	$2s^{1.13}2p^{0.14}4p^{0.12}$	$3s^{1.74}3p^{0.61}4p^{0.01}$
$LiMg_3^-$	−0.068	$2s^{0.75}2p^{0.29}3p^{0.03}$	$3s^{1.47}3p^{0.83}4p^{0.01}$
$LiMg_4^-$	0.014	$2s^{0.62}2p^{0.33}3p^{0.04}$	$3s^{1.39-1.59}3p^{0.54-0.95}4p^{0.01-0.02}$
$LiMg_5^-$	0.011	$2s^{0.58}2p^{0.37}3p^{0.04}$	$3s^{1.35-1.56}3p^{0.47-1.17}4p^{0.02-0.02}$
$LiMg_6^-$	0.064	$2s^{0.47}2p^{0.43}3p^{0.04}$	$3s^{1.24-1.41}3p^{0.69-1.21}4p^{0.01-0.03}$
$LiMg_7^-$	−0.139	$2s^{0.45}2p^{0.65}4p^{0.03}$	$3s^{1.26-1.43}3p^{0.43-1.05}4p^{0.01-0.03}$
$LiMg_8^-$	−0.102	$2s^{0.32}2p^{0.76}3p^{0.02}$	$3s^{1.19-1.27}3p^{0.76-1.05}4p^{0.01-0.03}$
$LiMg_9^-$	0.402	$2s^{0.38}2p^{0.16}3p^{0.05}$	$3s^{1.09-1.17}3p^{0.72-1.29}4p^{0.02}$
$LiMg_{10}^-$	0.271	$2s^{0.30}2p^{0.31}3p^{0.10}$	$3s^{1.06-1.56}3p^{0.31-1.39}4p^{0.02-0.03}$
$LiMg_{11}^-$	0.288	$2s^{0.32}2p^{0.27}3p^{0.10}$	$3s^{1.03-1.42}3p^{0.30-1.34}4p^{0.02-0.03}$

3.5. Bonding characters

Since $LiMg_9^-$ has outstanding stability and symmetry, we can consider it as a magic structure for $LiMg_n^-$. To elucidate its bonding character, the molecular orbitals, multi-center bonds, and electron localization function (ELF) are studied. Firstly, several typical molecular orbitals (MO) and their energy levels are plotted in Fig. 4. There is some degeneracy of energy levels in $LiMg_9^-$ due to its high structural symmetry of C_{3v}. The 1S state is the lowest MO with orbital energy of −6.19 eV. Among three 1P MOs, a merged energy level of $1P_x/1P_y$ is 0.22 eV lower than $1P_z$. The 1D character contains three energy levels of −1.64 eV for $1D_{xy}/1D_{x^2-y^2}$, −1.62 eV for $1D_z^2$, and −1.46 eV for $1D_{xz}/1D_{yz}$. The HOMO of the $LiMg_9^-$ cluster shows a 2S state with orbital energy of −0.99 eV, which is 1.94 eV lower in energy than its LUMO. The LUMO is one of the seven 1F MOs, which has the $1F_z^3$ character, followed by a merged energy level of $1F_{xz}^2/1F_{yz}^2$, a merged energy level of $1F_{xyz}/1F_z$, a single level of $1F_y$, and a single level of $1F_x$. It is clear that the occupied MOs completely satisfy 20 valence electrons of closed-shell $1S^21P^61D^{10}2S^2$, which may be one reason for its excellent stability. In addition, for the $LiMg_9^-$ cluster, the compositions of given MO orbitals are tabulated in Table S2 (supplementary materials). One can find that there is a distinct sp hybridization in the said cluster due to considerable contributions of the s and p atomic orbitals in all of the MOs. Secondly, the multi-center bonds of $LiMg_9^-$ are studied by the AdNDP method[59] to elucidate further the bonding nature, of which 1c–2e and 2c–2e represent localized, but the rest denotes delocalized bond.

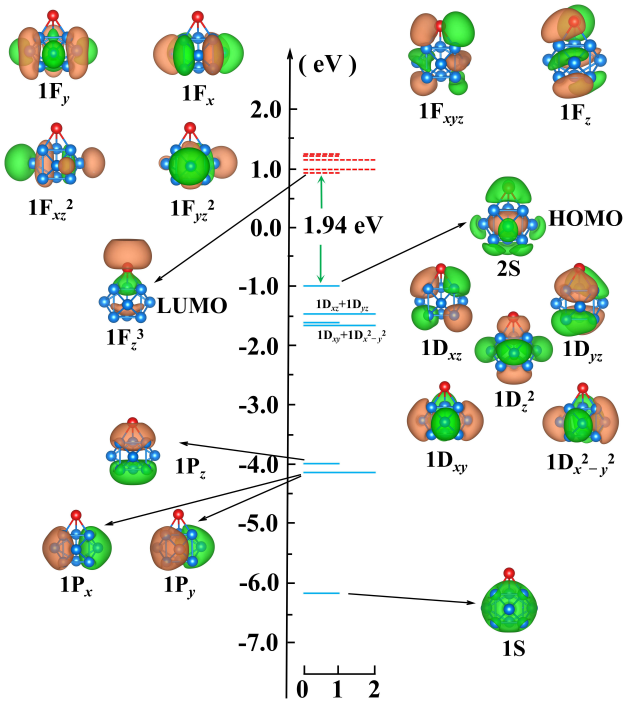


Fig. 4. Molecular orbitals and the corresponding energy levels of the $LiMg_9^-$ cluster. The HOMO–LUMO gap is indicated (in green).

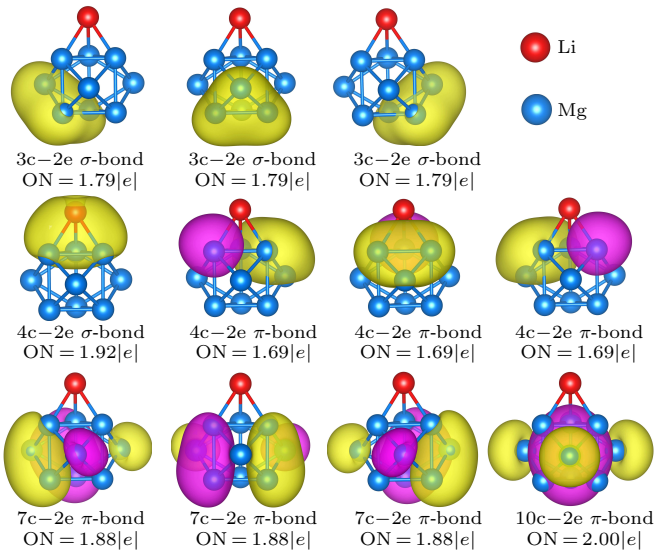


Fig. 5. The AdNDP chemical bonds of the $LiMg_9^-$ cluster (ON denotes the occupation number).

Consequently, the $LiMg_9^-$ cluster owns eleven delocalized bonds but no localized one, as shown in Fig. 5. There are three 3c–2e σ-type bonds with ON = 1.79$|e|$, produced by each Mg_3 ring in the bottom two and middle one Mg atoms. The 4c–2e σ-type bond with ON = 1.92$|e|$ reveals a strong interaction between Li and neighboring Mg atoms. The top three Mg atoms form three 4c–2e π-type bonds (ON = 1.69$|e|$) with each of the middle magnesium atoms. Three 7c–2e π-type bonds with ON = 1.88$|e|$ come from the Mg_3 ring in the middle as well as the top and bottom two Mg atoms. All the atoms generate one 10c–2e π-type bond with ON = 2.00$|e|$ in the $LiMg_9^-$ cluster. Finally, as shown in Fig. 6, the ELF is used to reflect the bonding intensity of the $LiMg_9^-$ cluster. Compare the colors of different regions, one can find that the value between Li and the neighboring Mg is relatively larger than that of other regions, indicating stronger Li–Mg interaction in $LiMg_9^-$.

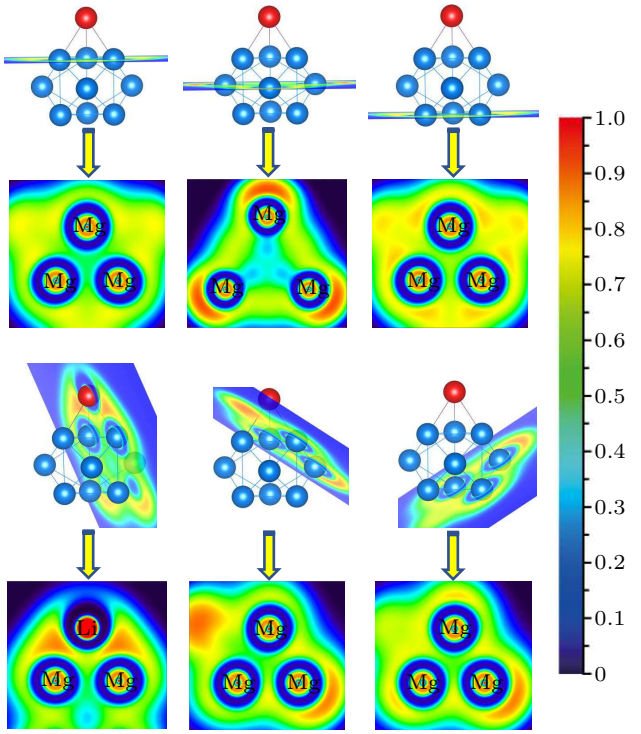


Fig. 6. The ELF of the $LiMg_9^-$ clusters.

3.6. Infrared (IR) and Raman spectra

For the most stable $LiMg_n^-$, we simulate their infrared and Raman spectra because the results can provide information on vibrational patterns and can be used to identify cluster structures by comparing experimental and theoretical spectra. As shown in Fig. 7, there is no imaginary frequency in the IR spectra of $LiMg_n^-$, which means all the structures are indeed stable. For all of the doped clusters, the IR and Raman vibrations are in the low-frequency region of 0–300 cm^{-1}. To identify the vibration mode of the characteristic peaks, the corresponding schematic diagrams of them are shown in Table S3 (supplementary materials). Note that the highest frequencies of IR and Raman spectra are caused by the stretching motion of the Li atom for all the $LiMg_n^-$ clusters. As a result, this motion contributes to several characteristic peaks in IR of the $LiMg_2^-$, $LiMg_3^-$, $LiMg_7^-$, $LiMg_{10}^-$, and $LiMg_{11}^-$ as well as those in Raman spectra of the $LiMg_4^-$, $LiMg_5^-$, $LiMg_6^-$, and $LiMg_9^-$ clusters, respectively. Moreover, the strongest peak at 146.3 cm^{-1} in Raman spectrum of $LiMg_2^-$ relates to a stretching mode of the Mg_2 bond. The peak at 196.3 cm^{-1} of $LiMg_3^-$ is caused by the breathing mode of the Mg_3 triangle. The vibration mode of the two Mg atoms at the apex of the triangular bipyramid produces the characteristic peak (76.5 cm^{-1}) in

Raman of $LiMg_4^-$. In the IR spectrum of $LiMg_5^-$, the strongest peak corresponds to a bending mode. For the $LiMg_6^-$ cluster, the strongest peak at 186.6 cm^{-1} is caused by swing modes of Li–Mg bond in two different directions. A swing mode leads to the characteristic peak (112.7 cm^{-1}) in the Raman spectrum of $LiMg_7^-$. Among vibration modes of $LiMg_8^-$, the inclined downward vibration of the Li atoms causes the surrounding Mg atoms to follow, producing the two characteristic peaks. That at 187.0 cm^{-1} in IR of $LiMg_9^-$ is assigned to a breathing mode of the $LiMg_4$ unit. Although the characteristic peaks of 288.0 cm^{-1} and 292.5 cm^{-1} in IR spectra of $LiMg_{10}^-$ and $LiMg_{11}^-$ are caused by the Li atom of stretching motion, it is stretched away from the z-axis because of the attached magnesium atom. In the Raman spectrum of $LiMg_{10}^-$, the peak of 208.6 cm^{-1} is also from a breathing mode of the $LiMg_4$ unit. A breathing mode of the top Mg_3 triangle produces a peak of 207.5 cm^{-1} in the Raman spectrum of the $LiMg_{11}^-$ cluster.

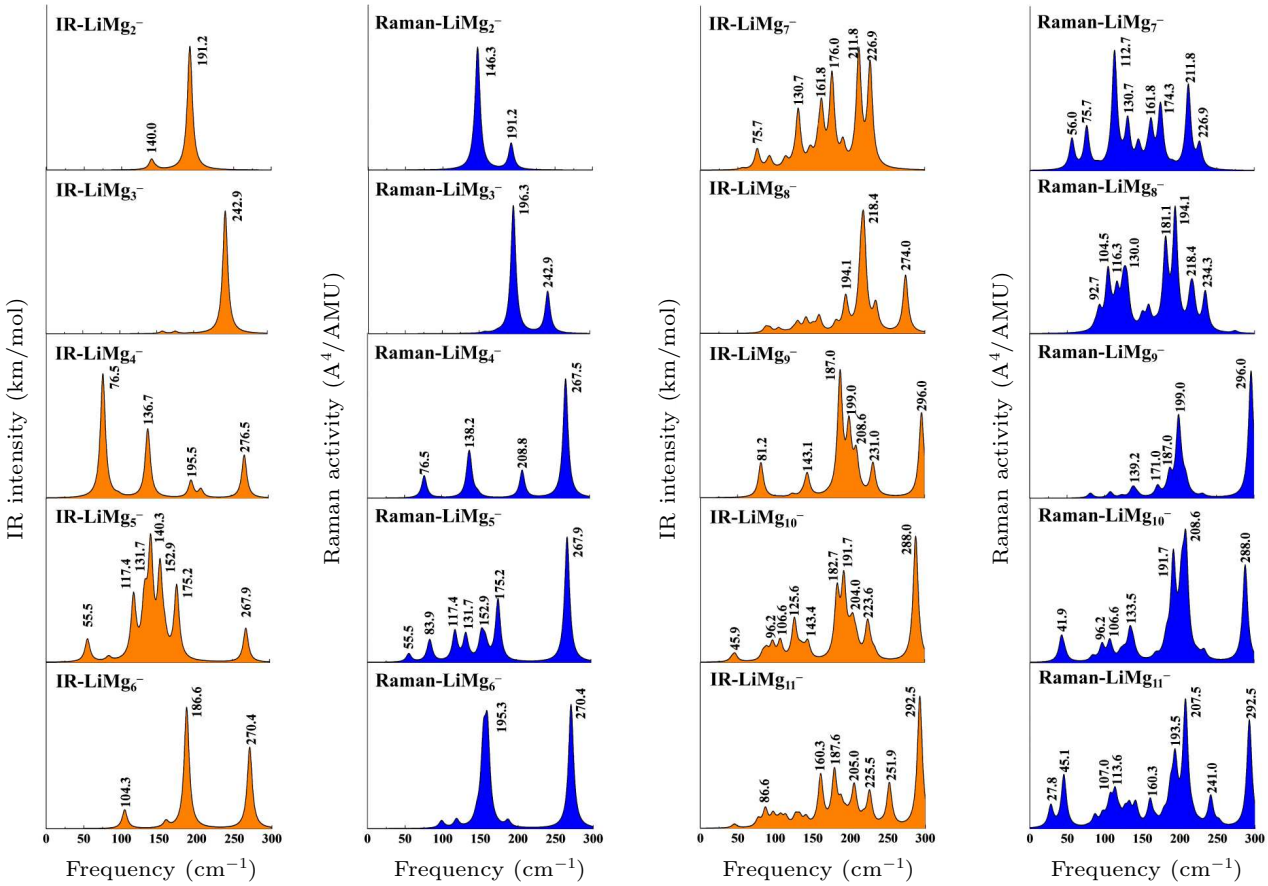


Fig. 7. IR and Raman spectra of the $LiMg_n^-$ ($n = 2$–11) clusters.

4. Conclusion

A systematic DFT study has been carried out to investigate the effect of lithium atom doping on the geometries, stabilities, and properties of Mg_n cluster anions. Global minima of $LiMg_n^-$ ($n = 2$–11) are searched through the PSO algorithm. It is clear that the doped Li atoms have a weak effect on the structure of the host clusters because most of the $LiMg_n^-$ clusters have the identical structure as the Mg_{n+1}^- clusters. However, the stabilities are significantly enhanced due to the doping of Li atoms. The convex position is the Li atom's favorite site in all doped clusters. Simulated PES of $LiMg_n^-$ could be viewed as a fingerprint for identifying cluster structures in the experiment. The stability parameters of the average binding energy, fragmentation energy, second-order energy difference, and HOMO–LUMO gaps indicate $LiMg_9^-$ is the most stable cluster. Molecular orbitals and bonding nature analysis carry out that the outstanding stability of $LiMg_9^-$ is related not only to a closed-shell $1S^21P^61D^{10}2S^2$ electronic configuration but also to more strong Li–Mg bonds caused by sp hybridization. Furthermore, most of the characteristic peaks in IR and Raman spectra are caused by the stretching motion of the Li atom in the $LiMg_n^-$ clusters.

Acknowledgments

Project supported by the National Natural Science Foundation of China (Grant No. 11404008), the Innovation Training Program for College Students of Shanxi Province of China (Grant No. S201910721061), and the Innovation Training Program for College Students of Baoji University of Arts and Sciences (Grant No. 20191XJ087).

References

[1] Du Y X, Sheng H T, Astruc D and Zhu M Z 2020 *Chem. Rev.* **120** 526
[2] Zhao J J, Du Q Y, Zhou S and Kumar V 2020 *Chem. Rev.* **120** 9021
[3] Peng F, Song X Q, Liu C, Li Q, Miao M S, Chen C F and Ma Y M 2020 *Nat. Commun.* **11** 5227
[4] Farooq U, Naz S, Xu H G, Yang B, Xu X L and Zheng W J 2020 *Coord. Chem. Rev.* **403** 213095
[5] Tian Y H, Sun W G, Chen B L, Jin Y Y and Lu C 2019 *Chin. Phys. B* **28** 103104
[6] Yan L J, Shao J M and Li Y Q 2020 *Chin. Phys. B* **29** 125101
[7] Li J, Zhai H J and Wang L S 2003 *Science* **229** 864
[8] Bergeron D E, Castleman J A W, Morisato T and Khanna S N 2004 *Science* **304** 84
[9] Sarkar U and Blundell S A 2009 *Phys. Rev. B* **79** 125441
[10] Jia Y H, Zhang H Y, Cheng L J and Luo Z X 2021 *J. Phys. Chem. Lett.* **12** 5115
[11] Zhang X X, Wang Y, Wang H P, Lim A, Gantefoer G, Bowen K T, Reveles J U and Khanna S N 2013 *J. Am. Chem. Soc.* **135** 4856
[12] Diederich T, Döppner T, Braune J, Tiggesbäumker J and Meiwes-Broer K H 2001 *Phys. Rev. Lett.* **86** 4807
[13] Thomas O C, Zheng W J, Xu S J and Bowen J K H 2002 *Phys. Rev. Lett.* **89** 213403
[14] Jellinek J and Acioli P H 2002 *J. Phys. Chem. A* **106** 10919
[15] Acioli P H and Jellinek J 2002 *Phys. Rev. Lett.* **89** 213402
[16] Duanmu K, Roberto-Neto O, Machado F B C, Hansen J A, Shen J, Piecuch P and Truhlar D G 2016 *J. Phys. Chem. C* **120** 13275
[17] Xia X X, Kuang X Y, Lu C, Jin Y Y, Xing X D, Merino G and Hermann A 2016 *J. Phys. Chem. A* **120** 7947
[18] Heidari I, De S, Ghazi S M, Goedecker S and Kanhere D G 2011 *J. Phys. Chem. A* **115** 12307
[19] Janecek S, Krotscheck E, Liebrecht M and Wahl R 2011 *Eur. Phys. J. D* **63** 377
[20] De S, Ghasemi A A, Willand A, Genovese L, Kanhere D and Goedecher S 2011 *J. Chem. Phys.* **134** 124302
[21] Knight W D, Clemenger K, de Heer Saunders W A, Chou M Y and Cohen M L 1984 *Phys. Rev. Lett.* **52** 2141
[22] Chen X F, Zhang Y, Qi K T, Li B, Zhu Z H and Sheng Y 2010 *Chin. Phys. B* **19** 033601
[23] Li J, Liu X Y, Zhu Z H and Sheng Y 2012 *Chin. Phys. B* **21** 033101
[24] Xi S G, Li Q Y, Hu Y F, Yuan Y Q, Zhao Y R, Yuan J J, Li M C and Yang Y J 2022 *Chin. Phys. B* **31** 016106
[25] Li Q Y, Xi S G, Hu Y F, Yuan Y Q, Zhao Y R, Li M C, Yuan J J and Yang Y J 2021 *Comput. Mater. Sci.* **197** 110605
[26] Zhu B C, Deng P J, Guo J and Kang W B 2022 *Front. Chem.* **10** 870985
[27] Zhu B C, Bao L, Deng P J, Zeng L, Kang W B and Guo J 2022 *J. Chem. Phys.* **157** 114303
[28] Medel V M, Reveles J U, Khanna S N, Chauhan V, Sen P and Castleman A W 2011 *Proc. Natl. Acad. Sci. USA* **108** 10062
[29] Ge G X, Han Y, Wan J G, Zhao J J and Wang G H 2013 *J. Chem. Phys.* **139** 174309
[30] Ma X L, Liu S G and Huang S P 2017 *Int. J. Hydrog. Energy* **42** 24797
[31] Zhao Y R, Xu Y Q, Chen P, Yuan Y Q, Qian Y and Li Q 2021 *Results Phys.* **26** 104341
[32] Peng X, Liu W C, Wu G H, Ji H and Ding W J 2022 *J. Mater. Sci. Technol.* **99** 193
[33] Ma X C, Jin S Y, Wu R Z, Wang J X, Wang G X, Krit B and Betsofen S 2021 *Trans. Nonferr. Matel. Soc.* **31** 3228
[34] Rao B K and Jena P 1988 *Phys. Rev. B* **37** 2867
[35] Fantcci P, Bonačić-Koutechỳ W P and Koutechỳ J 1989 *J. Chem. Phys.* **91** 4229
[36] Deshpande M, Dhavale A, Zope R R, Chacko S and Kanhere D G 2000 *Phys. Rev. A* **62** 063202
[37] Li C G, Cui Y Q, Tian H, Shao Q Q, Zhang J, Ren B Z and Yuan Y Q 2021 *Comput. Mater. Sci.* **200** 110800
[38] Liu S H, Qi Y J, Jin Y Z, Wang Y Y, Liu C, Yang H and Zhang Z X 2022 *Comput. Mater. Sci.* **210** 111440
[39] Wang Y C, Lv J, Zhu L and Ma Y M 2010 *Phys. Rev. B* **82** 094116
[40] Lv J, Wang Y C, Zhu L and Ma Y M 2012 *J. Chem. Phys.* **137** 084104
[41] Tong Q C, Lv J, Gao P Y and Wang Y C 2019 *Chin. Phys. B* **28** 106105
[42] Zhao Y R, Bai T T, Jia L N, Xin W, Hu Y F, Zheng X S and Hou S T 2019 *J. Phys. Chem. C* **123** 28561
[43] Lu C, Gong W G, Li Q and Chen C F 2020 *J. Phys. Chem. Lett.* **11** 9165
[44] Li C G, Li H J, Cui Y Q, Tian H, Shao Q Q, Zhang J, Zhao G, Ren B Z and Hu Y F 2021 *J. Mol. Liq.* **339** 116764
[45] Zeng L, Wei X F, Liang M K, Deng P J, Bi J and Zhu B C 2020 *Comput. Mater. Sci.* **182** 109795
[46] Li Z, Zhao Z, Zhou Z H, Wang H B and Li S L 2017 *Mater. Chem. Phys.* **199** 585
[47] Dou X L, Kuang X Y, Sun W G, Jiang G, Lu C and Hermann A 2021 *Phys. Rev. B* **104** 224510
[48] Peng F, Yao T S, Liu H Y and Ma Y M 2015 *J. Phys. Chem. Lett.* **6** 2363
[49] Li C G, Cui Y Q, Tian H, Ren B Z, Li Q Y, Li Y Y and Yang H 2022 *Nanomaterials* **12** 1654
[50] Jin W Y, Sun W G, Kuang X Y, Lu C and Kou L Z 2020 *J. Phys. Chem. Lett.* **11** 9643
[51] Frisch M J, Trucks G W, Schlegel H B, *et al.* 2009 *Gaussian 09 Revision D.01* (Wallingford CT: Gaussian Inc.)
[52] Gordon M S, Binkley J S, Pople J A, Pietro W J and Hehre W J 1982 *J. Am. Chem. Soc.* **104** 2797
[53] Mclean A D and Chandler G S 1980 *J. Chem. Phys.* **72** 5639
[54] Krishnan R, Binkley J S, Seeger R and Pople J A 1980 *J. Chem. Phys.* **72** 650
[55] Lu T and Chen F W 2012 *J. Comput. Chem.* **33** 580
[56] Koopmans T 1943 *Physica* **1** 104
[57] Lyalin A G, Semenov S K, Solov'yov A V and Cherepkov N A 2000 *J. Phys. B* **33** 3653
[58] Lyalin A G, Matveetsev A, Solov'yov I A and Solov'yov A V 2003 *Eur. Phys. J. D* **24** 15
[59] Zubarev D Y and Boldyrev A I 2008 *Phys. Chem. Chem. Phys.* **10** 5207